Mon. Not. R. Astron. Soc. **000**, 1–7 (2015) Printed 17 May 2015 (MN LaTeX style file v2.2)

Pulsar Lensing Geometry

Siqi Liu[1,3]⋆, Ue-Li Pen[1,2]†, J-P Macquart[4]‡, Walter Brisken[5]§, Adam Deller[6]¶

[1] *Canadian Institute for Theoretical Astrophysics, University of Toronto, M5S 3H8 Ontario, Canada*
[2] *Canadian Institute for Advanced Research, Program in Cosmology and Gravitation*
[3] *Department of Astronomy and Astrophysics, University of Toronto, M5S 3H4, Ontario, Canada*
[4] *ICRAR-Curtin University of Technology, Department of Imaging and Applied Physics, GPO Box U1978, Perth, Western Australia 6102, USA*
[5] *National Radio Astronomy Observatory, P.O. Box O, Socorro, NM 87801, USA*
[6] *ASTRON, the Netherlands Institute for Radio Astronomy, Postbus 2, 7990 AA, Dwingeloo, The Netherlands*

17 May 2015

ABSTRACT

We analyze archival data on PSR B0834+06, concluding that for this example the plasma lenses can be precisely modelled using the (Pen & Levin 2014) inclined sheet model, resulting in two distinct lens planes. This data strongly favours the grazing sheet model over turbulence as the primary source of pulsar scattering. The simple 1-D structure of the lenses opens up the possibility of using interstellar lenses as precision probes for pulsar lens mapping, and new opportunities for removing scattering.

A global conformal distance degeneracy exists which allows a rescaling of the absolute distance scale. This degeneracy is broken if the pulsar resides in a binary system, which is the case for most precision timing targets.

Key words: Pulsar

1 INTRODUCTION

Pulsars have long provided a rich source of astrophysical information due to their compact emission and predictable timing. One of the weakest measurements for most pulsars is their direct geometric distance. For some pulsars, timing parallax or VLBI parallax has resulted in direct distance determinations. For most pulsars, the distance is a major uncertainty for precision timing interpretations, including mass, moment of inertia, and gravitational wave direction (Boyle & Pen 2012).

Direct VLBI observation of PSR B0834+06 shows multiple images lensed by the interstellar plasma. Combining the angular positions and scintillation delays, the authors published the derived effective distance (Brisken et al. 2010) of approximately 1168 ± 23 pc for apexes whose time delays range from 0.1 ms to 0.4 ms, and 1121 ± 59 pc for 1 ms apexes. This represents a precise measurement compared to all other attempts to derive distances to this pulsar. This effective distance is a combination of pulsar-screen and earth-screen distances, and does not allow a separate determination of the individual distances. A binary pulsar system would in principle allow a breaking of this degeneracy (Pen & Levin 2014). One potential limitation is the precision to which the lensing model can be understood. In this paper, we demonstrate that the lensing screen consists of nearly parallel linear refractive structures, in two screens. The precise model confirms the one dimensional nature, and thus the small number of parameters that need to be measured to quantify the lensing screen.

2 LENSING

2.1 Archival data of B0834+06

Our analysis is based on the apex data selected from the secondary spectrum of pulsar B0834+06 in (Brisken et al. 2010), which was observed as part of a global VLBI project on 2005 November 12. Information from each identified apex includes delay τ, delay rate (differential frequency f_D), relative Right Ascension $\Delta\alpha$, relative declination $\Delta\delta$, error of $\Delta\alpha$ σ_α and error of $\Delta\delta$ σ_δ. Data of each apex are collected from four dual circular polarization 8 MHz wide sub-bands spanning the frequency range 310.5–342.5 MHz.

We divide the apex data with negative differential frequency into two groups: in one group time delay ranges from 0.1 ms to 0.4 ms, which we call 0.4 ms group, and in the other group time, delay at about 1 ms, which we call 1 ms group. The statistics of the positions of the points are: for 0.4 ms group, there are 10 apexes in the first two sub-bands, and 14 apexes in the last two sub-bands; for 1 ms group, there

⋆ E-mail: sqliu@cita.utoronto.ca
† E-mail: pen@cita.utoronto.ca
‡ E-mail:J.Macquart@curtin.edu.au
§ Email:wbrisken@aoc.nrao.edu
¶ E-mail:deller@astron.nl

are 5, 6, 5 and 4 apexes in the four sub-bands subsequently, with center frequency $f_{\rm band} = 314.5, 322.5, 330.5$ and 338.5 MHz.

Next we want to select the same apexes from four sub-bands. To match the same apexes in different sub-bands, we convert the differential frequency in different sub-bands to the one in 322.5 MHz, by $f_D/f_{\rm band} \cdot 322.5$ MHz. We map a total of 9 apexes from the 0.4 ms group, and 5 apexes from the 1 ms group. This results in an estimation for the average value in $f = 322.5$ MHz and standard deviation among four sub-bands. They are listed in Table 1. The f_D and τ are the arithmetic mean value of the four sub-bands. The mean value of $\Delta\alpha$ and $\Delta\delta$ are the weighted mean. The angular offset of the scintillation image away from the central emission is calculated as $\theta^2 = (\Delta\alpha\cos(\delta))^2 + (\Delta\delta)^2 - \sigma^2_{\Delta\alpha} - \sigma^2_{\Delta\delta}$.

The method we use to calculate the error of time delay τ, differential frequency f_D, $\Delta\alpha$ and $\Delta\delta$ are listed in Table 1, is by following equation:

$$\sigma^2_{\tau,\rm f_D,\Delta\alpha,\Delta\delta} = \frac{\sum\limits_{i=1}^{4}(x_i-\bar{x})^2}{n(n-1)}, \tag{1}$$

and $n = 4$ for four sub-bands.

2.2 One lens model

2.2.1 Distance of the lens

In the absence of a lens model, the fringe rate, delay and angular position cannot be uniquely related. To interpret the data, we adopt the lensing model of (Pen & Levin 2014). In this model, the lensing is due to projected fold caustics of a thin sheet closely aligned to the line of sight.

The relation of the distance of the pulsar D_p, the time delay τ with the angular offset θ, and the relation of velocity and the differential frequency f_D are described by the following equations:

$$\begin{aligned} \tau &= \frac{D_{\rm e}\theta^2}{2c}, \\ f_D &= f\frac{\rm d\tau}{\rm dt}, \end{aligned} \tag{2}$$

where $D_{\rm e}$ is the effective distance. If we denote the distance of the pulsar $D_{\rm p}$, the distance of the lens $D_{\rm s}$, then the effective distance is equivalent to the distance of the lens placed at the middle point of the pulsar: $D_{\rm e} = D_{\rm p}D_{\rm s}/(D_{\rm p} - D_{\rm s})$.

We plot the values of θ vs square root of τ in Figure 1. A least square analysis of the effective distance follows:

$$\begin{aligned} k\cdot\sum_{i=1}^{n}\frac{1}{\sigma^2_{ki}} &= \sum_{i=1}^{n}\frac{\theta/\sqrt{\tau}}{\sigma^2_{ki}}, \\ \frac{1}{\sigma^2_k} &= \sum_{i=1}^{n}\frac{1}{\sigma^2_{ki}}, \end{aligned} \tag{3}$$

where k is denoted as the slope in Figure 1, and σ_{ki} as the error of the slope. $\sigma_{ki} = \sigma_{\theta i}/\sqrt{\tau}$, $\sigma_\theta = \sqrt{(\sigma_{\Delta\alpha}\cos(\delta))^2 + \sigma^2_{\Delta\delta}}$. $n = 9$ for 1 ms group, and $n = 4$ for 0.4 ms group.

From this θ–$\sqrt{\tau}$ relation, the effective distance can be calculated as $D_{\rm e} = 2c/k^2$. Thus, $D_{\rm 1e} = 1023 \pm 27$ for the 0.4 ms group, distance of lens 1, and $D_{\rm 2e} = 1281 \pm 82$ for the 1 ms group, distance of lens 2. The errors, and uncertainties on the error, precludes a definitive interpretation of the apparent difference in distance. At face value, this indicates that the lens 1 is closer to the pulsar, and we will use this as a basis for the model in this paper. We discuss consequences of alternate interpretations in section 2.4. We take $D_{\rm 1e} = 1023$ pc, combined with the VLBI measured distance of the pulsar 640 pc, the distance of lens 1 D_1, where 0.4 ms scintillation points are refracted, is equal to 393.7 pc. For 1 ms apexes, the distance of lens 2 is equal to 426.7 pc. Lens 2 is closer to the pulsar, thus,the degeneracy of the distance of the screen is broken.

2.2.2 Angular positions of 0.4 *ms group*

We plot the observed relative angular positions in Figure 2. We fit a line to the angular positions of the 0.4 ms group, which has an positive angle of $\gamma = -25.2^\circ$ (east of the declination axis). We use this axis to define $\parallel$ and define $\perp$ by a 90° clockwise rotation from it.

We calculate θ from the θ–$\sqrt{\tau}$ relation and observed τ. Because all of the θ here lie on the axis defined by γ on lens 1, so they are also denoted $\theta_{1\parallel}$ listed in the first column in Table 1. Then the calculated angular positions of the 0.4 ms group are calculated:

$$\begin{aligned} \Delta\alpha_C &= -\theta\cdot\sin\gamma/\cos\delta, \\ \Delta\delta_C &= -\theta\cdot\cos\gamma, \end{aligned} \tag{4}$$

which are marked out with the scatter points on the left side in Figure 2.

2.2.3 Discussion of one lens model

The 0.4 ms group lens solution appears consistent with the premise of the inclined sheet lensing model (Pen & Levin 2014).

The time in last column of Table 1, which we denote as t_0, is calculated with $-2\tau f/f_D$, equivalent to pulsar moving at 640 pc plane from the original position to the lensed image position with the calculated velocity of the pulsar in that direction in one lens model.

That is one lens model fitting. Knowing time delay τ, we can calculate the distance of the screen; knowing the angular position of point 5 and its differential frequency f_D, we can get the velocity of the pulsar; knowing the velocity and observation differential frequency, we can get the position of points 1–4.

2.3 Double lens model

2.3.1 Solving the double lens model

We denote the position of the pulsar point A, position of the lensed image on lens 2 point H, position of the lensed image on lens 1 point B, position of the observer point O, pedal from the pulsar to line HJ point J, the pedal from point H to line BD point F, and the pedal from point B to line HJ point G, for easier discussion. Because points $1-4$ share the approximately same time delay with point 5, the lens where the image formed should be at the same distance away from us. The only reasonable position of screen (line HJ) that fits all these five points, marked with a solid line in Figure 2. That is unrealistic for the structure of the interstellar medium.

$\theta_{1\parallel}$(mas)	f_D(mHz)	τ(ms)	$\Delta\alpha$(mas)	$\Delta\delta$(mas)	t_0(days)
-8.26	-12.9(2)	0.0845(5)	2.9(3)	-8.2(4)	-48.7
-10.68	-16.8(3)	0.1412(9)	3.9(6)	-10.6(4)	-62.8
-12.32	-18.9(2)	0.188(2)	5.1(6)	-10.6(6)	-74.2
-13.41	-20.4(5)	0.222(3)	5.6(3)	-11.73(8)	-81.4
-13.82	-21.2(6)	0.236(2)	5.1(4)	-12.6(5)	-83.3
-14.59	-22.3(5)	0.2633(3)	6.2(3)	-14.2(7)	-88.1
-16.24	-24.6(4)	0.327(3)	6.5(6)	-14.1(4)	-99.0
-16.52	-24.9(4)	0.3378(3)	8.3(4)	-14.4(8)	-101
-17.39	-26.1(4)	0.3743(6)	8.5(3)	-15.7(3)	-107
···	-35.1(5)	0.950(2)	-15(1)	-21(1)	-202
···	-38.3(6)	0.9763(9)	-15(1)	-20.7(3)	-190
···	-40.2(6)	1.005(8)	-14(1)	-22.3(4)	-187
···	-41.3(5)	1.037(3)	-11(1)	-19(3)	-188
···	-43.1(4)	1.066(5)	-8(3)	-24(2)	-185

Table 1. 0.4 ms and 1 ms observation data and calculated data. The upper part of the table list the 0.4 ms group data, while the 1 ms group lie in the lower part of the table. Observation data include the differential frequency f_D, time delay τ from scintillation measurement (τ_1 for 0.4 ms group and τ_2 for 1 ms group); $\Delta\alpha$ and $\Delta\delta$ are from the VLBI measurement. The methods of how to calculate the error of time delay, differential frequency and the last column time are mentioned in Section 2.1.

Therefore, we consider another model candidate: the double lens model. Respective calculation shows that the light is first refracted by lens 2 and then refracted by lens 1.

The first step is to calculate the position of J. We make an estimate of the distance of J by the 1 ms θ–$\sqrt{\tau}$ relation, and then we calculated the position of J by matching the time delay of point 2 and point 5. The result shows that lens 2 is 426.7 pc away from us. And its position is marked in Figure 2. Because J is the pedal to lens 2, we made a line that is perpendicular to AJ, the solid line in Figure 2 to denote lens 2.

The second step is to find the matched pairs of those two lenses. By trial and error, we found that the 5 points in 0.4 ms group that have the largest θ should be the candidates where lens 1 lie. These five matched lines are marked with dot dash lines in Figure 2 and their values are listed in the first two columns in Table 3. They are the located at a distance 393.7 pc away from us. Here we define three distances:

$$\begin{aligned} D_{p2} &= 640 \text{ pc} - 426.7 \text{ pc} = 213.3 \text{ pc}, \\ D_{21} &= 426.7 \text{ pc} - 393.7 \text{ pc} = 33.0 \text{ pc}, \\ D_1 &= 393.7 \text{ pc} - 0 \text{ pc} = 393.7 \text{ pc}, \end{aligned} \tag{5}$$

where D_{p2} is the distance from the pulsar to lens 2, D_{21} is the distance from lens 2 to lens 1, and D_1 is the distance from lens 1 to the observer.

Figure 3 and Figure 4 are examples of how light are being refracted on the first lens plane and the second lens plane. We specifically chose the point with $\theta_{1\parallel}$ equal to -17.39 mas, which is point 5 on lens 2 and point 6 on lens 1 as an example. We solve the solutions in double lens model by following equations:

$$\begin{aligned} \frac{\text{JH}}{D_{p2}} &= \frac{\text{HG}}{D_{21}}, \\ \frac{\text{FB}}{D_{21}} &= \frac{\text{BD}}{D_1}. \end{aligned} \tag{6}$$

The solved positions are plotted in Figure 2, and respective time delays and differential frequencies are listed in Table 3. For the error of time delay τ in double lens model, we use the following equation:

$$(\frac{\sigma_{\tau_i}}{\tau_{2i}})^2 = (\frac{\sigma_{\tau 1i}}{\tau_{1i}})^2 + (\frac{\sigma_{\tau 2i}}{\tau_{2i}})^2 + (\frac{\sigma_{\tau 2j}}{\tau_{2j}})^2, \tag{7}$$

where τ_1 and $\sigma_{\tau 1}$ represent the time delay and its error from the 0.4 ms group on lens 1, τ_2 and $\sigma_{\tau 2}$ represent the time delay and its error from respective 1 ms group on lens 2. And τ_{2j} is the τ_2 for the nearest point in reference in Table 3 and $\sigma_{\tau 2j}$ is its error: for point $i = 1, 3$, $j = 2$; for point $i = 4$, $j = 5$.

For the error of differential frequency f_D, we use the following equation:

$$(\frac{\sigma_{f_i}}{f_{Di}})^2 = (\frac{\sigma_{f_{Di}}}{f_{Di}})^2 + (\frac{\sigma_{f_{D2}}}{f_{D2}})^2 \tag{8}$$

where f_{D2} and $\sigma_{f_{D2}}$ are the differential frequency and its error of the point in the second row in Table 3. $i = 1, 3, 4, 5$ for the subscription.

2.3.2 Comparing calculated result in double lens model and observation

Comparing τ, we calculated time delay τ_M for these five points, and list the results in Table 3. For point 2 and 5, they fit perfectly because these are the two points that we use these to calculate the position of J; for the rest three points, all of the calculated results are still within 3σ region of the observation time delays.

To compare differential frequency f_D, we need to calculate the velocity of the pulsar and the velocity of the lens. We consider lens 1 to be relative static, both the velocity of the pulsar and the velocity of lens 2 mentioned later are the relative velocities to lens 1. To calculate the velocity of the pulsar, we need two components, the $v_\parallel$ in $\parallel$ direction, and $v_\perp$ in $\perp$ direction, which is defined in Section 2.2.2. For $v_\parallel$, we still use the velocity that is calculated in 0.4 ms group in one lens model, that is 179.8 km/s. For the velocity of lens 2, because it is a line, and we do not consider radial velocity, so it could only be in the direction of AJ. However, by calculation, the $\angle$DAH is 82° by calculation, that means

$v_\perp$ and $v_{\rm lens2}$ are nearly degenerate. In the following discussion, we consider lens 2 to be static and only take $v_\perp$ into account.

To calculate $v_\perp$, we choose the point 2, which has the smallest errorbar of differential frequency. In a time period of 6500 s, the $v_\perp$ is calculated to be 6.85 km/s, in the direction pointing from B to D, to make the calculated f_{D2} match the observation f_D. Thus the $v_{\rm tot}$ is solved to be 192.4 ± 5.0 km/s, with an angle $\epsilon = 4.34^\circ$ west of north. The velocity calculations are all listed in Table 2. The direction of the velocity is marked on the top of the star in Figure 2.

With this velocity of the pulsar, we calculate the differential frequency f_M of point 1,3,4 and 5. Results are listed in Table 3. The calculated results all lie in the $3-\sigma$ region of the observation data.

The reduced chi-square χ^2_ν for time delay τ is 1.5 for 3 degrees of freedom, resulting in the probability of $P < 0.10$, and the reduced chi-square χ^2_ν for differential frequency f_D is 2.0 for 4 degrees of freedom, resulting in the probability of $P < 0.20$.

However, if the lens 1 lines are not parallel, there is still possibility that the differential frequency lie within the error region. Take point 4 for example, γ should lie within the region $25^\circ.2000^{+0.0013}_{-0.0006}$.

2.3.3 Discussion of double lens model

For 1 ms group, lens 2 only images a subset of the lens 1 images. This could happen if lens 1 screen is just under the critical inclination angle, such that only 3σ waves lead to a fold caustic. If the lens 2 was at a critical angle, the chance of encountering a somewhat less inclined system is of order unity. More surprising is the absence of a single refraction image of the pulsar, which is expected at position J. This could happen if the maximum refraction angle is just below critical, such that only rays on the appropriately aligned double refraction can form images. We made a plot of the refraction angle β in the direction that is transverse to the first lens plane in Figure 5. We denote the time that the lensed image on lens 2 to move from point H to point J, time t_1. From our calculation, 56 days before the lensed pulsar image to locate at J, it was at point 1; and 75 days before the lensed pulsar image to locate at J, it was at point 5. The data spans about 10% in frequency, making it unlikely that single lens image J would not be seen due to the larger required refraction angle. Instead, we speculate that the fold caustic could have formed near double lens image 1, and thus only intersections with the closer lens plane caustic south of image 1 are double lensed.

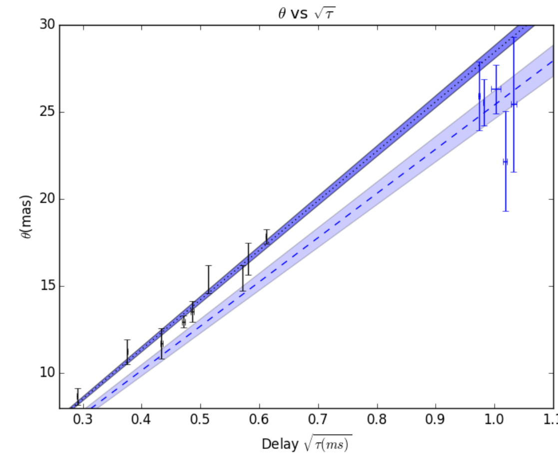

Figure 1. θ vs $\sqrt{\tau}$. Two separate lines through the origin were fitted to the points sampled among the 0.4 ms group and 1 ms group. The solid line is the fitted line of the 0.4 ms positions, where $k = -28.43$ with an error region of $\sigma_k = 0.37$. The dashed lines are the fitted lines of the 1 ms position, where $k = -25.40$ with an error region of $\sigma_k = 0.81$.

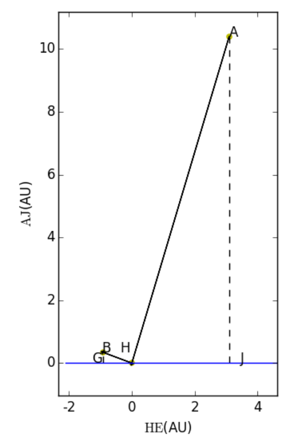

Figure 3. Refraction on lens 2. A is the position of the pulsar. H is the lensed image on lens 2. B is the lensed image on lens 1. J is the pedal of A to lens 2, and G is the pedal of B to lens 2. $v_{\rm JH}$ and $v_{\rm HG}$ should be equal, which is described in Section 2.3. In this case, $\theta_{1\|} = -17.39$ mas.

2.4 Distance Degeneracies

With two lens screens, the number of observables increases: in principle one could observe both single reflection delays and angular positions, as well as the double reflection delay and angular position. Three distances are unknown, equal to the number of observables. Unfortunately, these measurements are degenerate, which can be seen as follows. From the two screens $i = 1, 2$, the two single deflection effective distance observables are $D_{\rm 1e} \equiv c\tau_i/\theta_i^2 = D_i^2(1/D_i + 1/D_{pi})$. A third observable effective distance is that of screen 2 using screen 1 as a lens, $D_{\rm 21e} = D_1^2(1/D_1 + 1/D_{21})$, which is algebraically derivable from the first two relations: $D_{\rm 21e} = D_{\rm 1e}D_{\rm 2e}/(D_{\rm 2e} - D_{\rm 1e})$.

In this archival data set the direct single lens from the further plane at position J is missing. It would have been visible 56 days earlier. The difference in time delays to image J and the double reflection images would allow a direct determination of the effective distance to lens plane 2. Due to the close to 90 degree angle $\angle$DAJ between lenses, the effect would be about a factor of 10 ill conditioned. with sufficiently precise VLBI imaging one could distinguish if the double refracted images are at position B (if screen 1 is closer) or position H. As described above, we interpret the effective distances to place screen 2 further away.

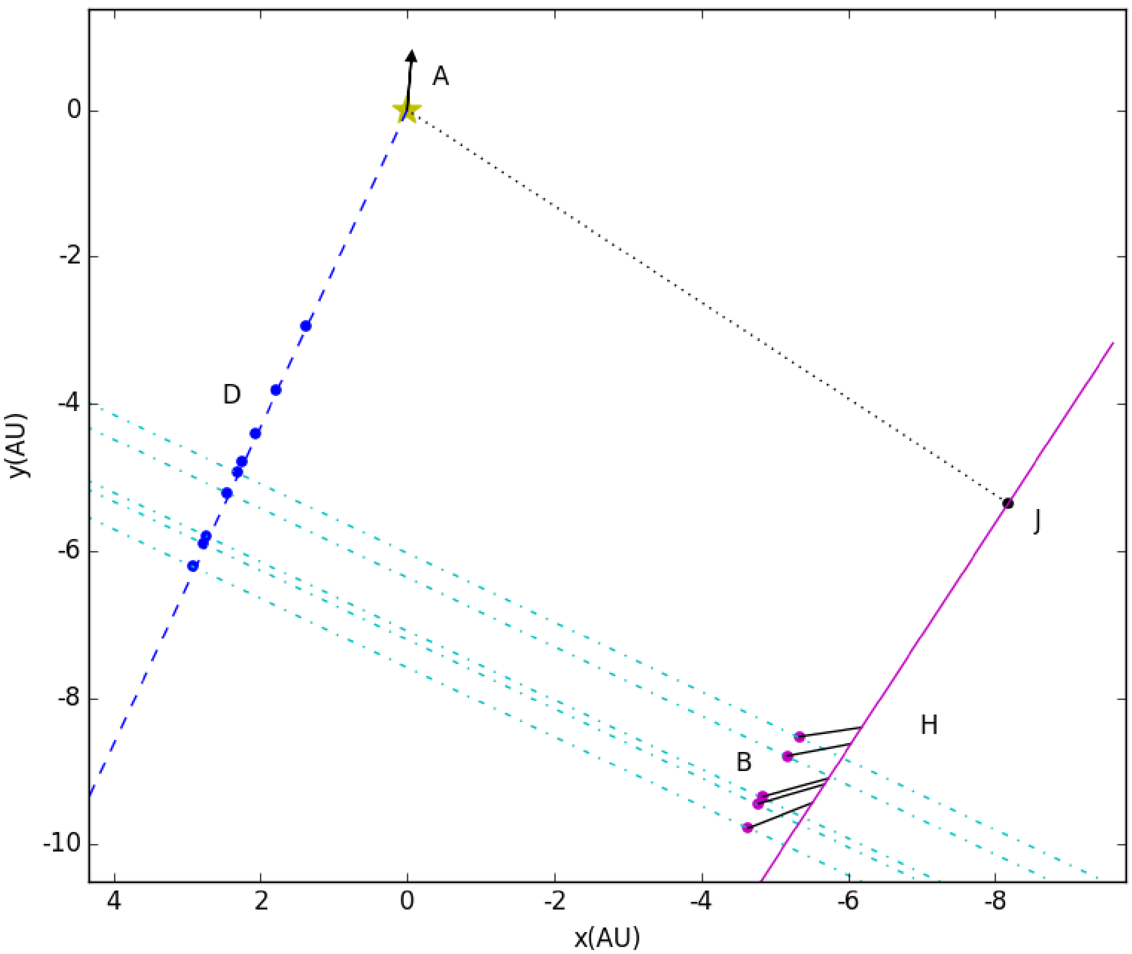

Figure 2. Observed and calculated angular positions of 0.4 ms and 1 ms data in double lens model. x axis and y axis are the relative distance to central emission of pulsar in Right Ascension direction and declination direction, on a 2D plane that is transverse to the line of sight. The position of the screen locate at 393.7 pc and 426.7 pc respectively. Scatter points on the left side, marked with letter D, are the calculated positions from the 0.4 ms apexes observation. Dash line is the fitted line of 0.4 ms apexes positions, with a angle $\gamma = -25.2°$ east of north. The scatter points on the right side, marked with letter B, are the calculated lensed image on lens 1 from 1 ms group. The short solid line connects the lensed image one lens 1(observable) and lensed image 2(unobservable), marked with letter H. Long solid line is the fitted line of these positions. The dotted line on the top right side is vertical to the solid line, and the pedal is called J. Short light solid lines connect the observation points and the calculated positions in 1 ms group. Middle dot dash lines connect the 0.4 ms and 1 ms calculated positions with the same $\theta_{1\|}$, which are denoted as lens 1. The proper motion of the pulsar is 192.4 km/s, with an angle $\epsilon = -4.34°$ east of north, is marked with an arrow from the star, point A the position of the pulsar, at the top of the figure.

Parameter	μ_α(mas/year)	μ_δ(mas/year)	μ_l(mas/year)	μ_b (mas/year)
calculated velocity of the pulsar to earth	-4.84 ± 0.12	63.4 ± 1.6	41.87 ± 1.06	60.09 ± 1.60
pulsar proper motion (relative to sun)	2.14 ± 0.21	51.64 ± 0.13	45.32 ± 0.49	46.51 ± 0.20
pulsar proper motion (relative to earth)	-7.52	53.5	28.99	52.1

Table 2. Summary of velocities in double lens model.

$\theta_{1\parallel}$ (mas)	τ_2(ms)	σ_τ(ms)	τ_M(ms)	f_D(mHz)	σ_f(mHz)	f_M(mHz)	t_1(days)
-13.82	0.9495	0.0094	0.9550	-35.1	0.81	-37.22	-56
-14.59	0.9763	0.00088	0.9763*	-38.3	0.64	-38.31†	-60
-16.24	1.005	0.011	1.027	-40.17	0.87	-40.64	-69
-16.52	1.0370	0.0059	1.0363	-41.27	0.88	-41.04	-70
-17.39	1.0663	0.0050	1.0663*	-43.08	0.84	-42.27	-75

Table 3. Comparison of time delay τ and the differential frequency f_D of the observation and the calculated result in double lens model. $\theta_{1\parallel}$ denotes the angular offset of lens 1. The values with star symbols on them are the points that we use to calculate the position of J and the point with a † symbol is the point that we use to calculate the velocity of the pulsar v_{A2}.

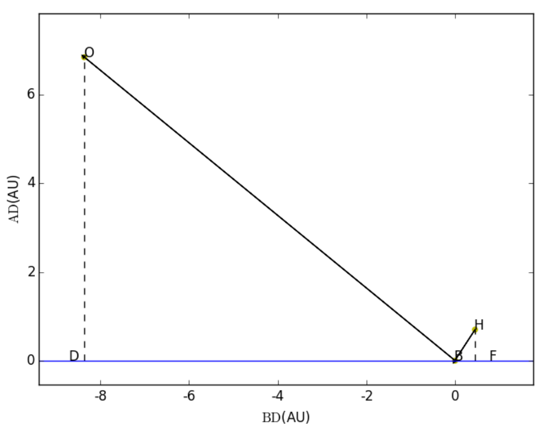

Figure 4. Refraction on lens 1. H is the lensed image on lens 2. B is the lensed image on lens 1. O is the position of the observer. F is the pedal of H to lens 2, and D is the pedal of O to lens 2. $v_{\rm FB}$ and $v_{\rm BD}$ should be equal, which is described in Section 2.3. In this case, $\theta_{1\parallel} = -17.39$ mas.

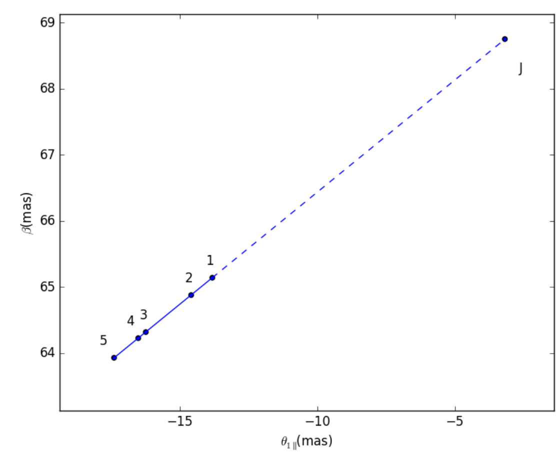

Figure 5. (π-$\angle$AHB) vs $\theta_{1\parallel}$. β_J is calculated with J as the lensed image on lens 2, when $\theta_{1\parallel} = -3.19$ mas.

3 POSSIBLE IMPROVEMENTS

We discuss several strategies which can improve on the solution accuracy. The single biggest improvement would be to monitor over a week, when the pulsar crosses each individual lens, including both lensing systems.

Angular resolution can be improved using longer baselines, for example adding a GMRT-GBT baseline doubles the resolution. Observing at multiple frequencies over a longer period allows for a more precise measurement: when the pulsar is between two lenses, the refraction angle β is small, and one expects to see the lensing at higher frequency, where the resolution is higher, and distances between lenses positions can be measured to much higher accuracy.

Holographic techniques (Walker et al. 2008; Pen et al. 2014) may be able to measure delays, fringe rates, and VLBI positions substantially more accurately. Combining these techniques, the interstellar lensing could conceivably achieve distance measurements an order of magnitude better than the current published effective distance errors. This could bring most pulsar timing array targets into the coherent timing regime, enabling arc minute localization of gravitational wave sources, lifting any potential source confusion.

Ultimately, the precision of the lensing results would be limited by the fidelity of the lensing model. In the inclined sheet model, the images move along fold caustics. The straightness of these caustics depends on the inclination angle, which in turn depends on the amplitude of the surface waves.

4 CONCLUSIONS

We have applied the (Pen & Levin 2014) inclined sheet model to archival apex data of PSR B0834+06. The data is well fit by two linear lensing screens, with nearly plane-parallel geometry. This appears a natural consequence of very smooth reconnection sheets, and are an unlikely outcome of ISM turbulence. These results, if extrapolated to multi-epoch observations of binary systems, this might result in accurate distance determinations and opportunities for removing scattering induced timing errors.

5 ACKNOWLEDGEMENTS

We thank NSERC for support.

REFERENCES

Boyle L., Pen U.-L., 2012, Phys. Rev. D, 86, 124028
Brisken W. F., Macquart J.-P., Gao J. J., Rickett B. J., Coles W. A., Deller A. T., Tingay S. J., West C. J., 2010, ApJ, 708, 232
Pen U.-L., Levin Y., 2014, MNRAS, 442, 3338
Pen U.-L., Macquart J.-P., Deller A. T., Brisken W., 2014, MNRAS, 440, L36
Walker M. A., Koopmans L. V. E., Stinebring D. R., van Straten W., 2008, MNRAS, 388, 1214